Characterization of Cement-Based Materials Using Diffuse Ultrasound

Jens Becker[1]; Laurence J. Jacobs, M.ASCE[2]; and Jianmin Qu[3]

Abstract: The objective of this research is to develop a quantitative understanding of the propagation of ultrasonic waves in cement-based materials by examining specimens made of a portland cement-paste matrix and glass bead ''aggregate.'' The incident ultrasonic waves are broadband and contain wavelengths on the order of the glass bead scatterers. Experimentally measured ultrasonic waves are interpreted using diffusion theory to quantitatively measure dissipation and diffusion coefficients as functions of frequency and microstructure. These results provide a basic understanding of the effect of some features of the microstructure on the propagation of ultrasonic waves, as well as supplying a first step in the characterization of distributed damage using ultrasonic methodologies.

DOI: 10.1061/(ASCE)0733-9399(2003)129:12(1478)

CE Database subject headings: Portland cement; Ultrasonic tests; Diffusion coefficient; Microstructures.

Introduction

Previous researchers (e.g., Evans et al. 1978) have been successful in relating the attributes of ultrasonic waves (such as attenuation) with specific microstructure parameters (like grain size) in ceramic and metallic materials, but there has been limited success in similar applications to cement-based materials. Experimental determination of attenuation and dispersion are difficult tasks in cement-based materials, mainly because of the scattering due to the randomly distributed aggregate, and the very high attenuation.

Several critical types of damage in cement-based materials are distributed throughout the material, and this damage can have a relatively small length scale—a few millimeters and smaller. This length scale, which can be on the order of (or smaller than) the aggregate, dictates the use of higher frequencies (hundreds of kilohertz and higher) for accurate flaw detection. Examples of deleterious interactions leading to this type of damage includes: freeze-thaw, intrusion of water and acids, alkali-silica reaction (ASR), and even dynamic loading. Since the damage can be of a similar size as the aggregate, traditional ultrasonic evaluation methods have difficulty in differentiating between microstructure features (such as aggregate and porosity) and damage, because they all scatter the ultrasonic waves in similar ways.

[1]Graduate Research Assistant, School of Civil and Environmental Engineering, Georgia Institute of Technology, Atlanta, GA 30332-0355; current address: Institute A for Mechanics, Univ. of Stuttgart, D-70569 Stuttgart, Germany.

[2]Professor, School of Civil and Environmental Engineering, and G. W. Woodruff School of Mechanical Engineering, Georgia Institute of Technology, Atlanta, GA 30332-0355 (corresponding author). E-mail: laurence.jacobs@ce.gatech.edu

[3]Professor, G. W. Woodruff School of Mechanical Engineering, Georgia Institute of Technology, Atlanta, GA 30332-0405.

Note. Associate Editor: Eric N. Landis. Discussion open until May 1, 2004. Separate discussions must be submitted for individual papers. To extend the closing date by one month, a written request must be filed with the ASCE Managing Editor. The manuscript for this technical note was submitted for review and possible publication on February 20, 2003; approved on April 29, 2003. This technical note is part of the ***Journal of Engineering Mechanics***, Vol. 129, No. 12, December 1, 2003. ©ASCE, ISSN 0733-9399/2003/12-1478–1484/$18.00.

Selleck et al. (1998) examined the properties of freeze-thaw (combined with a salt pond) damaged concrete using time-domain ultrasonic pulses. Microscopic examination showed the presence of distributed microcracking, but experimentally measured changes in ultrasonic velocity and amplitude (500 kHz center frequency) did not conclusively identify the damage. Schickert (1998, 1999) performed dispersion and attenuation measurements in concrete in the frequency range of 150–800 kHz, correlating the attenuation with the grain size and porosity, while Jacobs and Owino (2000) used coherent ultrasonic signals (up to 1 MHz) to determine the effect of aggregate size on Rayleigh waves propagating in cement-based materials. Popovics et al. (2000) operated on pulse-echo signals with split-spectrum processing to decrease the noise level backscattered by the microstructure of the concrete.

Statistical methods, such as diffusion theory, can account for the random distribution of microcracks and aggregate. Consider for example, the work in fluid acoustics that analyzes the ultrasonic field in randomly distributed glass spheres immersed in water (e.g., Schriemer et al. 1997) or in solid media, such as aluminum foams (e.g., Weaver 1998). Note that the application to solids is inherently more complicated than fluid acoustics (or optics) because of the presence of two coupled wavefields and the practical difficulties in averaging high numbers of measurements. Anugonda et al. (2001) applied diffusion theory to concrete (in the 100–900 kHz range) to calculate diffusion parameters, but the variation in the calculated parameters is relatively high. They showed results for one type of concrete specimen, and did not investigate differences due to aggregate size and distribution on the measured diffusion parameters. Note that other researchers have used complementary approaches to the problem of scattering in fluid-saturated, porous media. Berryman (1985) used Biot's equations to develop a (frequency limited) solution to this problem, while Schwartz and Plona (1984) examined ultrasonic wave propagation in water-saturated, densely packed spherical scatterers using an effective media approximation.

The objective of the current research is to develop a quantitative understanding of the propagation of ultrasonic waves in cement-based materials by considering specimens made of a cement-paste matrix and glass bead ''aggregate'' with a variety of

Table 1. Specimen Specifications

Name	Diameter (mm)	Thickness (mm)	Beads diameter (mm)	Volume fraction (%)
1 mm loose	76	12.7–13.1	1	22
1 mm medium	76	14.3–15.5	1	32
1 mm dense	76	15.5–16.0	1	41
3 mm loose	76	12.0–12.9	3	22
3 mm medium	76	14.1–16.1	3	32
3 mm dense	76	16.5–17.5	3	41
Paste	76	15.5–16.5	no beads	0
Steel	76	16	—	—

sizes and distributions. The incident ultrasonic waves are broadband and contain wavelengths on the order of the glass bead scatterers. Experimentally measured waves are interpreted using diffusion theory to quantitatively measure dissipation and diffusion coefficients as functions of frequency and microstructure. These results provide a basic understanding of the effect of features of the microstructure (such as aggregate size and distribution) on the propagation of ultrasonic waves, as well as supplying a first step in the characterization of distributed damage using ultrasonic methodologies.

Ultrasonic Diffusion Approximation

An ultrasonic wavefield in a heterogeneous medium is the sum of a coherent *ballistic* field, and an incoherent *diffuse* field. The diffuse field is strongly scattered by the media—it is spatially incoherent, as well as incoherent in time with respect to the source—and its phase is (approximately) random. The ballistic field is spatially coherent, as well as being coherent with the source in time; it is either not scattered at all or forward scattered. Effective media theories and coherent potential approximation theories model the ballistic portion of a signal—the amplitudes of the ballistic field are significantly larger than the amplitudes of the diffuse field, so the diffuse field contribution is neglected in these theories. Ballistic theories give accurate results for either a small volume fraction of scatterers, or for long wavelengths compared to the scatterer size (i.e., low frequency), but break down in the strong scattering regime. In addition, these coherent field theories cannot separate attenuation caused by real energy losses (known as dissipation effects) from attenuation caused by scattering losses.

The diffusion approximation was first developed for optics, and a general model applicable to elastic waves is available, see Sheng (1995). Ultrasonic diffusion in a body is described by a second-order parabolic partial differential equation that describes the time evolution of the spectral energy density (energy per frequency, per volume)

$$\frac{\partial\langle E(x,t,f)\rangle}{\partial t} - D\Delta\langle E(x,t,f)\rangle + \sigma\langle E(x,t,f)\rangle = P(x,t,f) \quad (1)$$

where $E(x,t,f)$=spectral energy density (at time t and frequency f) at the point specified by the vector x and $\langle\cdot\rangle$ indicates the expected value with respect to the different configurations of the random media. $P(x,t,f)$=spectral source energy density; $D(f)$=frequency-dependent diffusion coefficient; and $\sigma(f)$=energy dissipation coefficient (frequency-dependent). The body is assumed to be isotropic—the diffusion coefficient is independent of direction—and all scattering is assumed to be linearly elastic (no energy loss during scattering). Eq. (1) predicts the ultrasonic spectral energy density in an average sense, and is similar to the heat transfer equation, but with an additional dissipation term.

Table 2. Typical Borosilicate Glass Properties

Property	Symbol	Value
Young's modulus	E	62.8GPa
Poisson's ratio	ν	0.2
Density	ρ	2,230 kg/m^3
Longitudinal wave speed	c_l	5,594 m/s[a]
Shear wave speed	c_s	3,425 m/s[a]

[a]Values are calculated from elastic properties.

The experimental setup used in this research dictates a radially symmetric solution of Eq. (1) in cylindrical coordinates (independent of the angle ϕ) with an impulse source at the origin, $P(r,t,f)=P_0\delta(t)\delta(r)$. The specimen thickness is small relative to the lateral dimensions, so the gradient in the z-direction is neglected and the lateral dimensions are assumed to be infinite ($r\to\infty$). This leads to a fundamental solution of Eq. (1) as (Carslaw and Jaeger 2000)

$$\langle E(r,t,f)\rangle = \frac{P_0}{4D\pi t} e^{-r^2/(4Dt)} e^{-\sigma t} \quad (2)$$

Experimental Procedure

Cement-based specimens are made with two sizes of borosilicate glass beads (1 and 3 mm diameter) and are mixed with cement-paste and cast in circular molds. The cement-paste is a mixture of portland ASTM Type I cement and water, with a water/cement ratio of 0.4 by mass. Note that 1.03% NaO_2 equivalent of lithium is added to the cement-paste to mitigate ASR and to prevent the associated cracking (see Kurtis et al. 2002 for a review of this reaction). A paste specimen is made with no glass beads and with no lithium added. A vibration table is used to remove entrapped air bubbles, the specimens are cured in a lime-water bath for at least 30 days, and the surfaces are polished. Each specimen has a circular shape with a diameter of 76 mm and thicknesses that vary from 14 to 16 mm. Table 1 summarizes the specimens, includes thickness values, and presents an identification scheme based upon bead size and volume fraction. *All specimens (besides the paste specimen) have the same absolute amount of cement-paste matrix material*. The volume fraction is calculated by dividing the glass volume by the specimen volume. A steel specimen (homogeneous at these ultrasonic wavelengths of a few millimeters and larger) is included for reference measurements.

The mechanical properties of the glass beads and the cement-paste are summarized in Tables 2 and 3. The glass beads are the

Table 3. Typical Cement-Paste Properties

Property	Symbol	Value
Young's modulus	E	16 GPa (19.5 GPa[a])
Poisson's ratio	ν	n.a. (0.26[a])
Density	ρ	1,945 kg/m^3
Longitudinal wave speed	c_l	3,530 m/s
Shear wave speed	c_s	1,990 m/s

[a]Values are calculated from wave speeds.

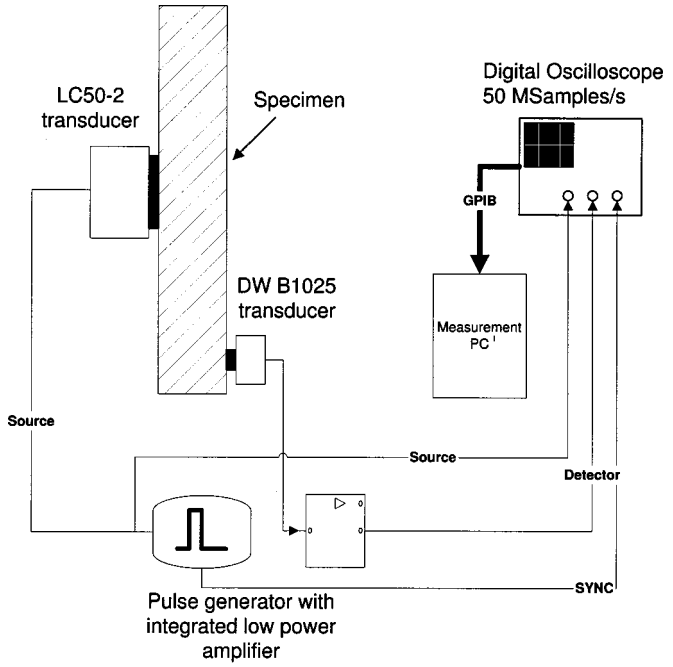

Fig. 1. Experimental setup for diffuse field measurement

scattering aggregate, but with a simplified spherical shape. The cement-paste matrix is viscoelastic and contains a random distribution of air voids (pores) that have a length scale orders of magnitude smaller than the glass beads (micrometer versus millimeter). In addition, there is an interfacial zone between the cement-paste matrix and the glass bead aggregate (Young et al. 1998) that can potentially cause additional dissipation losses (energy losses at an imperfect interface). If the actual dissipation is dominated by losses in the viscoelastic cement-paste matrix, as opposed to losses at the interfacial zone, then the measured dissipation will be dependent on the amount of cement-paste matrix in a specimen.

The experimental setup is shown in Fig. 1, with a Ultran LC50-2 source transducer, and a Digital Wave B1025 receiving transducer—the receiving transducer is mounted on a 1 mm diameter contact pad to enable point-like detection. Point-like detection is critical because the diffuse ultrasonic field cancels itself out on the transducer surface—this point-like detector measures the contribution of one coherent speckle. The bandwidth of the source/receiver transducer combination is from 0.3 to 2 MHz, see Becker (2002) for details. The impulse response of each of the specimens is measured off epicenter, on the opposite side (with respect to the source), at a location where no coherent signal components are measured. The diffuse field response is recorded with 60,000 record points at a 50 MHz sampling frequency, roughly corresponding to 1 ms of useful signal length. Only 600 μs of the signal is actually used for the diffusion calculations, although the signal's tail is useful to determine the noise level. The ratio of ultrasonic wavelength to glass bead scatterer diameter approximately varies from 0.7 to 13 in these experiments.

Experimental Results and Discussion

A typical time-domain signal (r of 30 mm, and measured in the 3 mm loose specimen as defined in Table 1) is shown in Fig. 2. Note that the spikes between -2 and 3 μs are artificial bleed-through from the trigger which are windowed out and not included in the analysis. The spectral energy density $\hat{E}(r,t,f)$ of a time-domain signal (at a particular frequency f and at the measurement point r) is calculated by performing a time-frequency analysis. This time-domain signal is divided into overlapping time windows of length Δt, these windows are multiplied with a Hanning window to smooth the signal edges (and reduce artificial side lobes), and then the discrete time Fourier transform of each individual time window is calculated. Finally, the spectral energy density, $\hat{E}(r,t,f)$, of each time window in a certain frequency band is calculated by summing the power spectrum in a bandwidth of width Δf centered around frequency f_c. Note that $\hat{E}(r,t,f)$ is not the ultrasonic spectral energy density itself, but differs from this value by a factor related to transducer efficiency, coupling effects, and the time-frequency analysis parameters—this factor is assumed to be an unknown constant (Weaver and Sachse 1995).

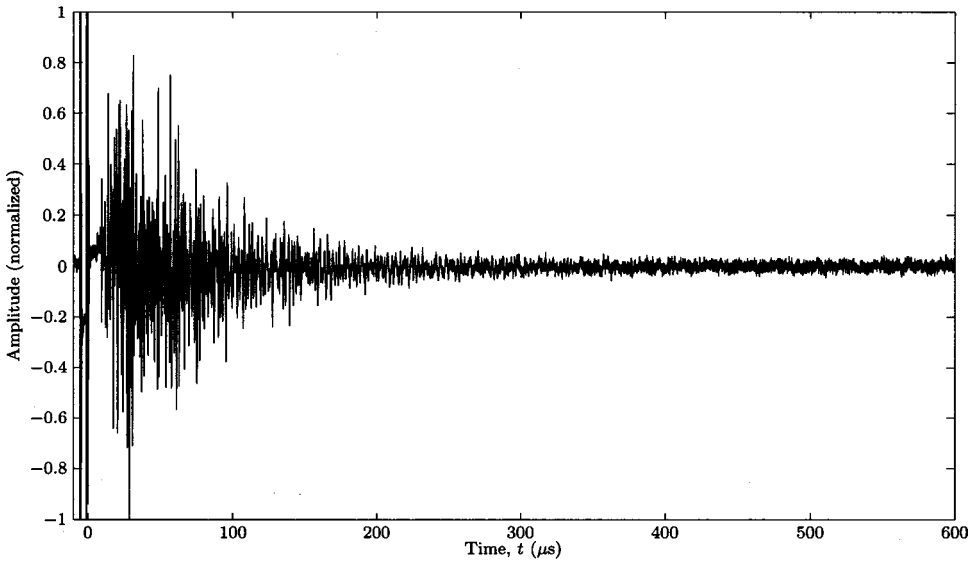

Fig. 2. Time-domain signal in 3 mm loose specimen

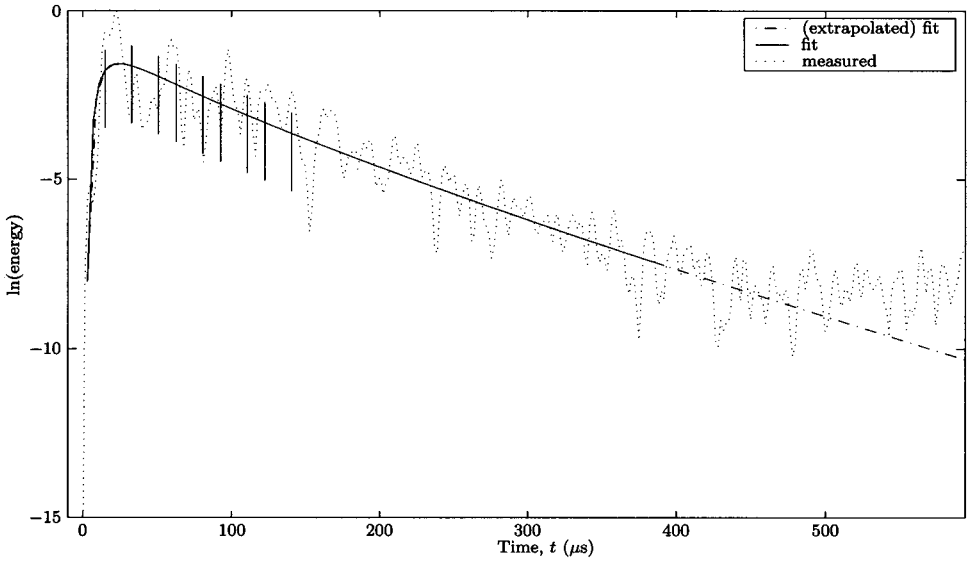

(a) f_c=0.3 MHz

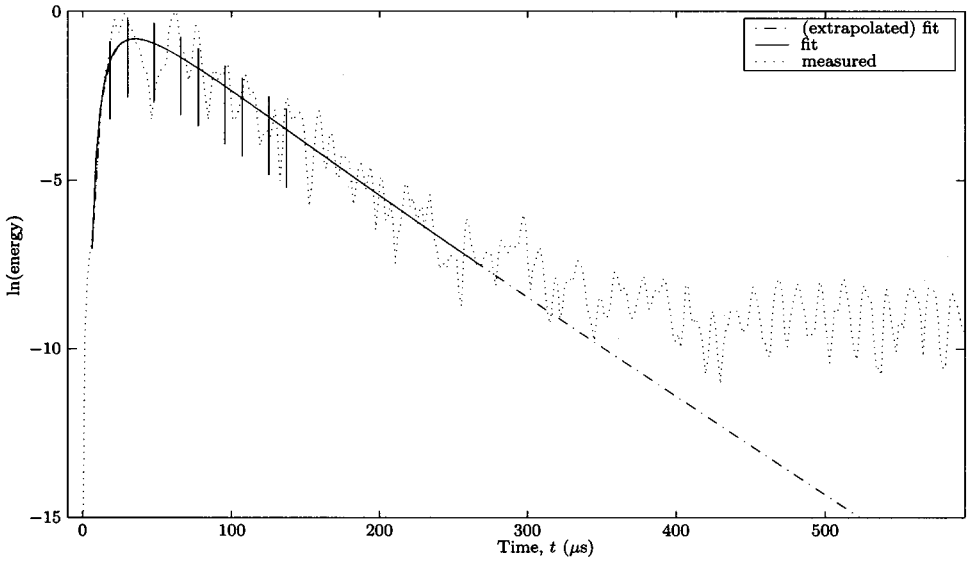

(b) f_c=0.6 MHz

Fig. 3. (a) Curve fits for 3 mm loose specimen, with expected deviation as bars—$f_c = 0.3$ MHz and (b) curve fits for 3 mm loose specimen, with expected deviation as bars—$f_c = 0.6$ MHz

Eq. (2) is a relationship for the *expected* value, $\langle E(r,t,f)\rangle$, of the spectral energy density. From probability theory, the best way to measure $\langle E(r,t,f)\rangle$ is to average values of $\hat{E}(r,t,f)$ that are measured in multiple, independent configurations; this average converges to $\langle E(r,t,f)\rangle$ if the configurations are statistically independent. Multiple, independent configurations can be obtained by taking another random realization of the distribution of the scatterers in the media (this is easily done in fluid acoustics) or by averaging measurements made at different spatial points r_i. Note that variability associated with transducer coupling makes measurements at multiple spatial points impractical, so the variance of only one measured curve $\hat{E}(r,t,f)$ with respect to $\langle E(r,t,f)\rangle$ is of interest, see Weaver and Sachse (1995) for details. The solution given by Eq. (2) is taken as an approximate model for $\langle E(r,t,f)\rangle$ at a certain frequency *f*. The diffusion and dissipation parameters *D* and σ plus the source term P_0 are recovered from the minimization of the square error

$$\epsilon = \sum_{t_i} \ln\langle E(r,t,f)\rangle - \ln \hat{E}(r,t,f))^2 \tag{3}$$

P_0 is a factor related to the amount of measured energy and measurement-related factors, and is not needed for the material characterization.

Examples of curve fits using Eq. (3) for different frequencies are shown in Figs. 3 and 4—the spectral energy density curves are calculated with $\Delta t = 6$ μs and $\Delta f = 0.3$ MHz from the time-domain signal of Fig. 2 and are shown on a logarithmic scale. The expected deviations, calculated with the predicted variance (Weaver and Sachse 1995), are superimposed as bars. These large deviations are not errors, but predicted fluctuations that are caused by the randomness of the media. Note that these deviations lie randomly above and below the curves, which suggests a good quality of fit. The early time range from 15–30 μs shows a worse prediction than at later times (see Figs. 3 and 4). This is

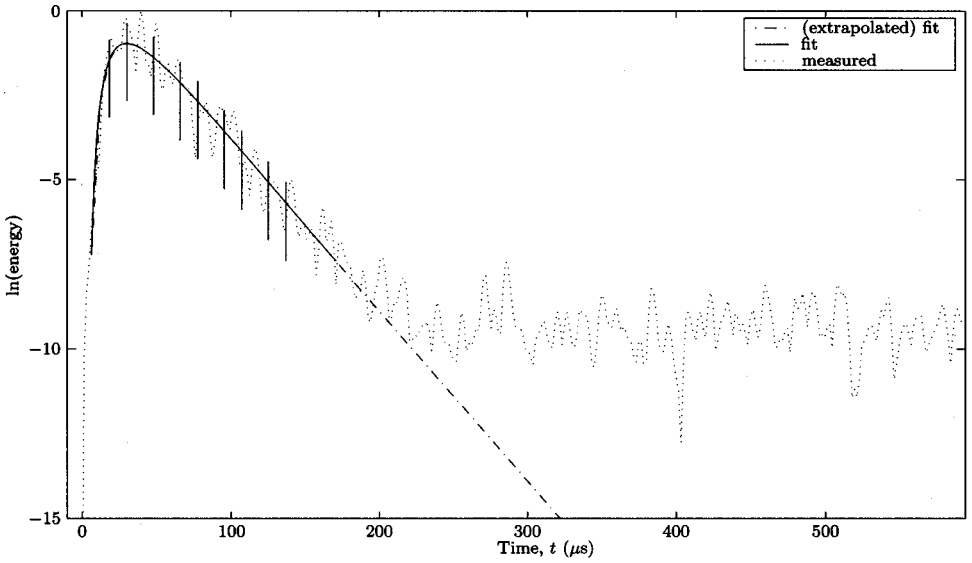

(a) f_c=1.3 MHz

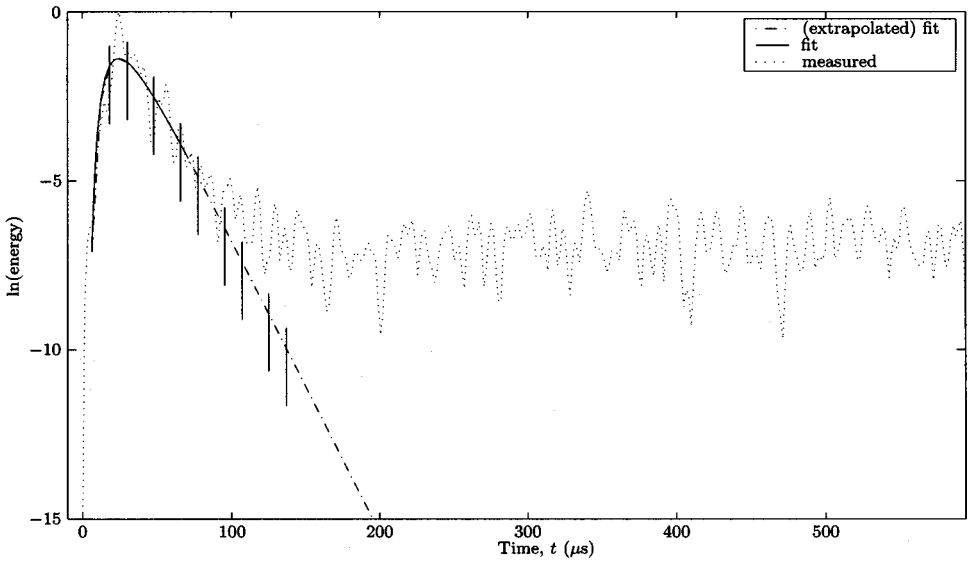

(b) f_c = 1.9 MHz

Fig. 4. (a) Curve fits for 3 mm loose specimen, with expected deviation as bars—$f_c = 1.3$ MHz and (b) curve fits for 3 mm loose specimen, with expected deviation as bars—$f_c = 1.9$ MHz

because only a few travel paths from the source to the receiver contribute to the measured field, so less implicit averaging takes place during these times, which results in higher deviations. This effect will mainly influence the calculation of the diffusion coefficient *D*.

First consider the energy dissipation coefficient σ as a function of frequency. Dissipation coefficients are determined (recovered) for all the specimens listed in Table 1, and are calculated with exactly the same time-frequency analysis parameters, time window of 6 μs, and frequency bandwidth of 0.3 MHz. There are no statistical differences between the σ values recovered from the loose, medium, and dense specimens of the same bead size, so ten different σ values for each bead type are averaged together (Becker 2002). Fig. 5(a) compares the recovered dissipation value, σ as a function of frequency and specimen type, with one-sigma standard deviation bars. Note that the standard deviation in the recovered dissipation values increases with frequency, especially above 1.5 MHz. All cement-based specimens seem to show dissipation with a linear frequency-dependence, a phenomena that is particularly important since dissipation (attenuation) due to viscoelastic material damping is linearly dependent on frequency (Rose 1999). A linear regression is performed on the σ parameter; Fig. 5(b) shows the linear regression for frequencies 0.25–1.25 MHz and these regression lines approximately go through the origin. The paste specimen has the highest recovered dissipation values, while the 1 and 3 mm bead specimens have lower dissipation values, and are virtually identical to each other. Finally, note that dissipation in the steel specimen [the curve is near the bottom of Fig. 5(a)] is substantially lower than all the cement-based specimens.

The almost equal dissipation values for the 1 and 3 mm bead specimens suggest that the energy dissipation in cement-based materials is only due to the viscoelastic cement-paste matrix, and not due to the interfacial zone. The ratio of the cement-paste

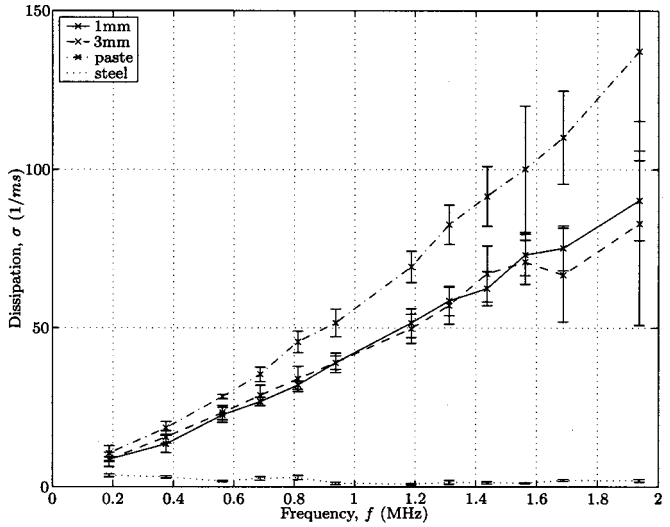

(a) Averaged, recovered dissipation, σ

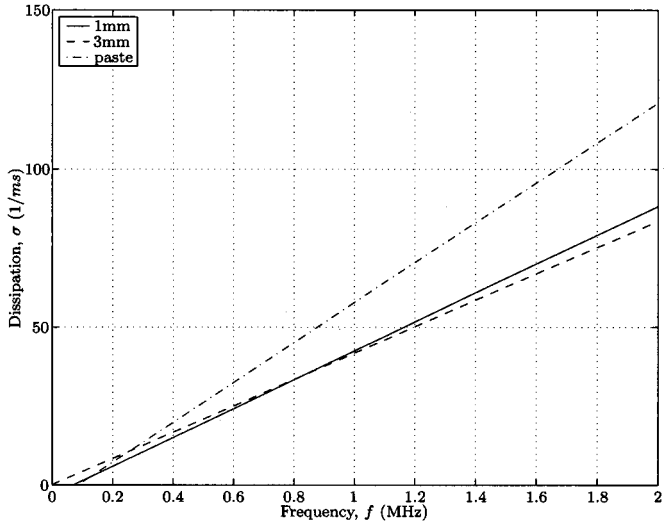

(b) Linear regression

Fig. 5. (a) Dissipation σ comparison for 3 mm, 1 mm, paste, and steel specimens—averaged, recovered dissipation σ and (b) dissipation σ comparison for 3 mm, 1 mm, and paste specimens—linear regression

volume in the paste specimen, to the cement-paste (matrix material) volume in the bead specimens is 1.56. This ratio is expected to be equal to the ratio of the dissipation values ($\sigma_{\text{paste}}/\sigma_{\text{bead}}$), as well as equal to the ratio of the dissipation slopes. This is confirmed by examining the slopes of the linear regressions in Fig. 5(b), where the ratio is equal to 1.7 for the 3 mm/paste, and 1.5 for the 1 mm/paste. If the interfacial zone influences dissipation (at least partly), σ is expected to scale with the surface area, i.e., by the factor 9 from 1 to 3 mm bead scatterers. This effect is not seen—the dissipation losses from the interfacial zone appear to be negligible compared to the high energy losses that occur in the cement-paste matrix.

Now consider diffusivity *D*. Again, there are no systematic differences found when comparing the *D*'s of the loose, medium, and dense specimens of the same bead size. To enable a comparison of the 1 mm, 3 mm, and paste specimens, seven to ten *D* coefficients recovered from individual 1 mm, 3 mm, and paste measurements are averaged and presented with one-sigma deviation bars in Figs. 6 and 7. These figures show a systematic pattern of lower diffusivity values for the 3 mm beads specimens, when compared to the 1 mm beads specimens. The higher diffusivity values for the 1 mm bead scatterers in comparison to the 3 mm beads is reasonable, and is in agreement with the expectation that the 3 mm beads lead to more scattering at lower frequencies, which in turn slows down the diffusion process (lower *D*). Above 1.5 MHz, the 1 and 3 mm bead specimen diffusivity values approach each other, which is expected since more scattering is also expected in the 1 mm bead specimens at these higher frequencies.

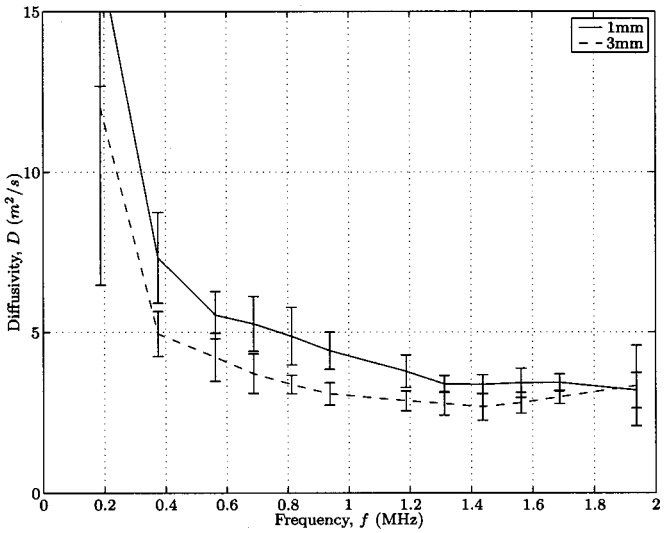

Fig. 6. Averaged diffusivity *D* of 3 and 1 mm bead specimens

Overall, it is possible to distinguish the two different bead sizes with the recovered diffusivity coefficient *D*. However, differences in volume fractions cannot be distinguished with the *D*'s recovered with the proposed methodology. The reason for this is most likely that *D* is weakly related to the volume fractions, so any differences are small and in the range of the measurement and processing error. Note the recovered diffusivity values presented in Figs. 6 and 7 for lower frequencies (below 0.9 MHz) are in the same range as those presented in Anugonda et al. (2001).

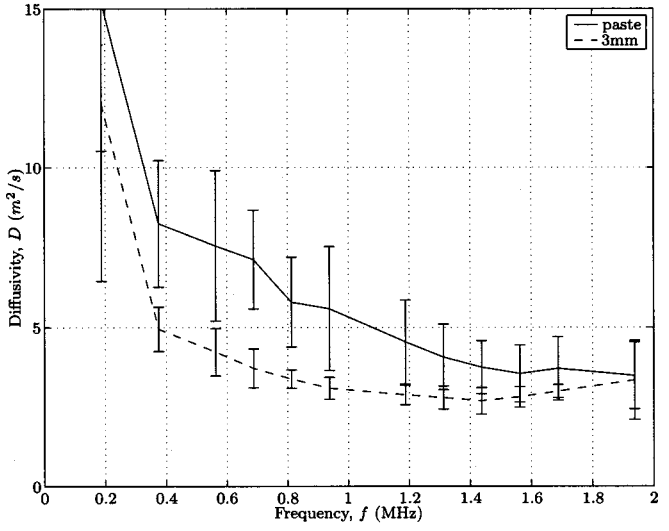

Fig. 7. Averaged diffusivity *D* of paste and 3 mm bead specimens

Conclusion

This research characterizes cement-based materials with diffuse ultrasound, and quantitatively measures dissipation and diffusion coefficients as functions of frequency and microstructure. These results demonstrate one advantage of using diffuse ultrasound in this application—the separation (uncoupling) of attenuation due to scattering losses, from attenuation due to material losses. The measured dissipation values (material losses) are realistic and are used to quantitatively characterize differences between paste and bead specimens. These results indicate that the dissipation process (material attenuation) in cement-based materials is dominated by losses in the viscoelastic cement-paste matrix, as opposed to losses at the interfacial zone. The measured diffusivity values (scattering losses) show qualitative trends, but the results are not as conclusive. Diffusivity appears to have a limited capability to resolve variations in microstructure, being more dependent on the parameters selected for the time-frequency analysis—this is not the case with the dissipation calculation, which is very insensitive to parameter selection. Note that a more accurate solution of the diffusion equation, Eq. (1), would lead to better D recovery, but such a closed-form solution that is suitable for curve fitting is not available.

The proposed method can experimentally resolve differences in features of the microstructure of a specimen, but is limited by theoretical shortcomings; a model is needed to predict the influence of scatterer size and distribution. However, these experimental diffusion results provide a basic understanding of the effect of microstructure on the propagation of ultrasonic waves in cement-based materials, and supply a first step in the characterization of distributed damage using ultrasonic methodologies.

Acknowledgments

This work is partially supported by the National Science Foundation through Grant No. CMS-0201283. The Deutscher Akademischer Austausch Dienst (DAAD) provided partial support to Jens Becker. The writers wish to thank Professor Kim Kurtis for her helpful discussions and Mr. Jason Ideker for preparing the specimens.

References

Anugonda, P., Wiehn, J. S., and Turner, J. A. (2001). ''Diffusion of ultrasound in concrete.'' *Ultrasonics*, 39, 429–435.

Becker, J. (2002). ''Investigation of the microstructure of heterogeneous materials using ultrasonic waves.'' MS thesis, School of Civil and Environmental Engineering, Georgia Institute of Technology, Atlanta.

Berryman, J. G. (1985). ''Scattering by a spherical inhomogeneity in a fluid-saturated porous medium.'' *J. Math. Phys.*, 26(6), 1408–1419.

Carslaw, H. S., and Jaeger, J. C. (2000). *Conduction of heat in solids*, Oxford University Press, Oxford, England.

Evans, A. G., Tittmann, B. R., Ahlberg, L., Khuri-Yakub, B. T., and Kino, G. S. (1978). ''Ultrasound attenuation in ceramics.'' *J. Appl. Phys.*, 49, 2669–2679.

Jacobs, L. J., and Owino, J. (2000). ''Effect of aggregate size on attenuation of Rayleigh surface waves in cement-based materials.'' *J. Eng. Mech.*, 126(11), 1124–1130.

Kurtis, K. E., Collins, C. L., and Monteiro, P. J. M. (2002). ''The surface chemistry of the alkali-silica reaction: A critical evaluation and x-ray microscopy.'' *RILEM Concrete Science and Engineering, Special Issue on Alkali-Aggregate Reaction*, 4, 2–11.

Popovics, S., Bilgutay, N., Karaoguz, M., and Akgul, T. (2000). ''High-frequency ultrasound technique for testing concrete.'' *ACI Mater. J.*, 97(1), 58–65.

Rose, J. L. (1999). *Ultrasonic waves in solid media*, Cambridge University Press, Cambridge, England.

Schickert, M. (1998). ''Ein empirisches Modell der frequenzabhängigen Schallschwächung von Beton (Empirical model of frequency-dependent ultrasound attenuation in concrete).'' *Deutsche Gesellschaft für Zerstörungsfreie Prüfung, DGZfP* (German Society of Nondestructive Evaluation, Annual Meeting 1998, Weimar), 233–240 (in German).

Schickert, M. (1999). ''Ein empirisches Modell der Dispersion von Ultraschall in Beton (Empirical model of ultrasound dispersion in concrete).'' *Deutsche Gesellschaft für Zerstörungsfreie Prüfung, DGZfP* (German Society of Nondestructive Evaluation, Annual Meeting 1999, Celle), 559–566 (in German).

Schriemer, H. P., Cowan, M. L., Page, J. H., Sheng, P., Liu, Z., and Weitz, D. A. (1997). ''Energy velocity of diffusing waves in strongly scattering scattering media.'' *Phys. Rev. Lett.*, 79(17), 3166–3169.

Schwartz, L., and Plona, T. J. (1984). ''Ultrasonic propagation in close-packed disordered suspensions.'' *J. Appl. Phys.*, 55(11), 3971–3977.

Selleck, S. F., Landis, E. N., Peterson, M. L., Shah, S. P., and Achenbach, J. D. (1998). ''Ultrasonic investigation of concrete with distributed damage.'' *ACI Mater. J.*, 95(4), 27–36.

Sheng, P. (1995). *Introduction to wave scattering, localization and mesoscopic phenomena*, Academic, New York.

Young, J. F., Mindess, S., Gray, R. J., and Bentur, A. (1998). *The science and technology of civil engineering materials*, Prentice-Hall, Englewood Cliffs, N.J.

Weaver, R. L. (1998). ''Ultrasonics in an aluminum foam.'' *Ultrasonics*, 36, 435–442.

Weaver, R. L., and Sachse, W. (1995). ''Diffusion of ultrasound in a glass bead slurry.'' *J. Acoust. Soc. Am.*, 97, 2094–2102.